Symmetry blockade and its breakdown in energy equipartition of square graphene resonators

Yisen Wang, Zhigang Zhu, Yong Zhang, and Liang Huang

Citation: Appl. Phys. Lett. **112**, 111910 (2018); doi: 10.1063/1.5009492
View online: https://doi.org/10.1063/1.5009492
View Table of Contents: http://aip.scitation.org/toc/apl/112/11
Published by the American Institute of Physics

Symmetry blockade and its breakdown in energy equipartition of square graphene resonators

Yisen Wang,[1] Zhigang Zhu,[1] Yong Zhang,[2] and Liang Huang[1,a)]
[1]*School of Physical Science and Technology, and Key Laboratory for Magnetism and Magnetic Materials of MOE, Lanzhou University, Lanzhou, Gansu 730000, China*
[2]*Department of Physics, Xiamen University, Xiamen 361005, China*

(Received 17 October 2017; accepted 4 March 2018; published online 16 March 2018)

The interaction between flexural modes due to nonlinear potentials is critical to heat conductivity and mechanical vibration of two dimensional materials such as graphene. Much effort has been devoted to understanding the underlying mechanism. In this paper, we examine solely the out-of-plane flexural modes and identify their energy flow pathway during the equipartition process. In particular, the modes are grouped into four classes by their distinct symmetries. The couplings are significantly larger within a class than between classes, forming symmetry blockades. As a result, the energy first flows to the modes in the same symmetry class. Breakdown of the symmetry blockade, i.e., inter-class energy flow, starts when the displacement profile becomes complex and the inter-class couplings bear nonneglectable values. The equipartition time follows the stretched exponential law and survives in the thermodynamic limit. These results bring fundamental understandings to the Fermi-Pasta-Ulam problem in two dimensional systems with complex potentials and reveal clearly the physical picture of dynamical interactions between the flexural modes, which will be crucial to the understanding of their contribution in high thermal conductivity and mechanism of energy dissipation that may intrinsically limit the quality factor of the resonator. *Published by AIP Publishing*. https://doi.org/10.1063/1.5009492

Nano-electromechanical resonators (NEMS) based on two dimensional (2D) materials, such as graphene, have attracted extensive attention due to their low mass and high quality factors (Q factors).[1–4] The Fermi-Pasta-Ulam (FPU) physics[5] plays an important role in the performance of graphene resonators as the dissipation of the fundamental mode due to coupling with other modes intrinsically limits the Q factor of the device.[6] A key feature of a 2D material is that it bears the flexural (out-of-plane) modes, which plays an important role in the high heat conductivity[7] and the superior performance of mechanical vibrations.[1] To understand the anharmonic phonon-phonon scattering, it is critical to treat the interaction between these modes induced by the nonlinear potentials and identify the route to equipartition.[5,8,9] This has been investigated in 1D cases where for the FPU-β model, the energy flow pathway is obtained analytically based on the sine form of mode functions.[10] A different approach based on perturbation theory is also proposed.[11,12] While the analysis can be feasible for 1D lattices and when the nonlinear potential is simple, it is highly nontrivial to extend the methods to 2D systems,[13] especially for those with complex potentials such as graphene.

In this paper, we investigate exclusively the energy equipartition between the flexural modes, which is important for graphene nanomechanical resonators as the out-of-plane motion is their most dominant dynamics.[1,3,14,15] We have developed a numerical procedure to characterize the interaction between the modes due to nonlinear potentials. Our computation unveils completely the route and microscopic dynamics of thermalization. Interestingly, we found that the flexural modes are grouped into different classes based on their symmetry properties. The modes within each symmetry class have strong interactions, while the modes belonging to different symmetry classes have much weaker interactions. This forms the blockade for the energy flow due to the symmetry. Particularly, in the case where only one mode is excited initially, its energy will redistribute to the modes in the same symmetry class in a short time. While for modes in the other symmetry classes, it takes a substantially longer time for them to get energy, which occurs only when the interactions between these modes and the modes in the class that is first excited become large, as more and more modes get energy and the displacement profile becomes complex. For the cases that can reach equipartition, our extensive simulations confirm the stretched exponential form of relaxation time, which survives in the thermodynamic limit. Our results are of great theoretical significance and can also help to understand the role played by flexural modes in high thermal conductivity in graphene and the mechanism of energy dissipation that constrains the Q factor limits in graphene resonators.

We focus on a set of square graphene sheets with fixed boundaries [Fig. 1(a)]. The length of the graphene sheets varies from 2.7 nm to 16.8 nm with 11 different sizes, and the total number of carbon atoms is in the range of [296, 10 820]. We employ the valence force field (VFF) model considering the interatomic carbon sp^2 bond interactions[16–19] $U_{sp^2} = \sum_{i=1}^{N} \gamma \quad \mathbf{D}_i \cdot \mathbf{D}_i + \frac{1}{2}\sum_{i=1}^{N} \quad \sum_j \frac{\alpha}{4a_0^2}(\mathbf{r}_{ij}^2 - a_0^2)^2 + \sum_{i=1}^{N} \sum_{j<k} \frac{\beta}{a_0^2}(\mathbf{r}_{ij} \cdot \mathbf{r}_{ik} + \frac{1}{2}a_0^2)^2$, where N is the total number of the atoms, i is the atom index, and j and k are the i's nearest neighboring atoms. $\mathbf{r}_{ij}$ is the bond vector that connects atom i

a)Electronic mail: huangl@lzu.edu.cn

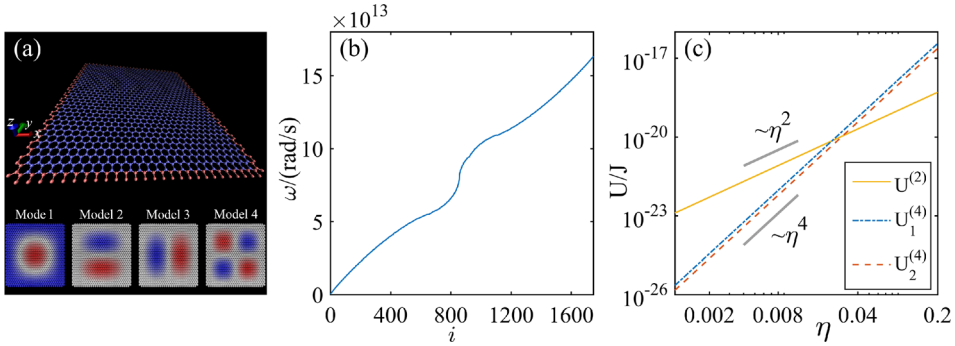

FIG. 1. (a) Configuration of the graphene sheet. The sheet is 6.9 nm by 7.4 nm, which contains 1992 carbon atoms in total and 1748 inner atoms that are able to move. The insets show the first four normal modes with different symmetries: symmetric-symmetric (SS), antisymmetric-symmetric (AS), SA, and AA with respect to x and y axes. Light gray (red) and black (dark blue) indicate maximum and minimum values of the normal modes, respectively. (b) The frequency spectrum versus mode number. The frequencies are ordered by increasing values. The minimum and maximum frequencies are 3.04×10^{11} rad/s (48.4 GHz) and 1.63×10^{14} rad/s (26.0 THz), respectively. (c) The potential terms $U^{(2)}$, $U_1^{(4)}$, and $U_2^{(4)}$ versus relative deformation η. The graphene sheet is deformed with the first normal mode.

to atom j. $a_0 = 1.421$ Å is the equilibrium bond length, and $\mathbf{D}_i = \sum_j \mathbf{r}_{ij}$ is the dangling bond vector. The parameters $\alpha = 155.9\,\mathrm{J/m^2}$, $\beta = 25.5\,\mathrm{J/m^2}$, and $\gamma = 7.4\,\mathrm{J/m^2}$ have the same dimension as the coefficient of stiffness.[16–19] The first term of the potential gives the energy cost necessary to change the angle between p_z-orbitals, which are approximately normal to the graphene surface. The last two terms represent the energy cost necessary to change the length and angle between covalent C-C bonds.

To address the effect of flexural modes and in accordance with the motion of graphene resonators, we consider only the z-direction motion. The VFF model can be simplified as $U_{sp^2} = \sum_{i=1}^{N} \gamma(\sum_j z_j - 3z_i)^2 + \frac{1}{2}\sum_{i=1}^{N}\sum_j \frac{\alpha}{4a_0^2}(z_j - z_i)^4 + \sum_{i=1}^{N}\sum_{j<k}\frac{\beta}{a_0^2}[(z_j - z_i)(z_k - z_i)]^2 = U^{(2)} + U_1^{(4)} + U_2^{(4)}$, where z_i is the z-displacement of site i from its equilibrium position. It is clear that $U^{(2)}$ is the second order potential, which corresponds to the linear interaction, while $U_1^{(4)}$ and $U_2^{(4)}$ are the fourth order potentials. Therefore, the z direction vibration of the graphene system can be effectively an FPU-β model in the hexagonal lattice.

The force acting on the ith atom is given by $F_i = -\frac{\partial U}{\partial z_i} = \sum_n -\frac{\partial U^{(n)}}{\partial z_i} = -\sum_n \frac{1}{n-1}\sum_j \frac{\partial^2 U^{(n)}}{\partial z_i \partial z_j} z_j \equiv \sum_j V_{ij}^{(n)} z_j$, where $V_{ij}^{(n)} = -\frac{1}{n-1}\frac{\partial^2 U^{(n)}}{\partial z_i \partial z_j}$ and n is the order of the potential term. The equation of motion can be written as $m\mathbf{z} = \mathbf{V}^{(2)} \cdot \mathbf{z} + \mathbf{V}^{(4)} \cdot \mathbf{z}$, where $\mathbf{z} = [z_1, \ldots, z_N]^T$ is the vector of displacement in the z-direction, and $\mathbf{V}^{(2)} = [V_{ij}^{(2)}]_{N\times N}$ and $\mathbf{V}^{(4)} = [V_{ij}^{(4)}]_{N\times N}$ correspond to linear and nonlinear force fields and can be derived from $U^{(2)}, U_1^{(4)}$, and $U_2^{(4)}$, respectively. Specifically, $\mathbf{V}^{(2)}$ is given by $V_{mn}^{(2)} = -24\gamma$ if $n=m$, 12γ if $n=m$'s nearest neighbor, -2γ if $n=m$'s next nearest neighbor, and 0 otherwise. $\mathbf{V}^{(4)}$ can be obtained numerically from $U_1^{(4)}$ and $U_2^{(4)}$. Let $\{\lambda_i, \varphi_i, i = 1, \ldots, N\}$ be the set of eigenvalues and eigenvectors of $\mathbf{V}^{(2)}$, i.e. $\mathbf{V}^{(2)}\varphi_i = \lambda_i \varphi_i = -m\omega_i^2 \varphi_i$, then φ_i will be the normal mode of the system with eigenfrequency $\omega_i = \sqrt{-\lambda_i/m}$. For a given configuration $\mathbf{z}$ such that $\mathbf{z} = \sum_j c_j \varphi_j$, where c_j are the normal coordinates, denote $\mathbf{c} = [c_1, \ldots, c_N]^T$, we have

$$m\ddot{\mathbf{c}}(t) = \mathbf{\Lambda} \cdot \mathbf{c}(t) + \mathbf{S}(t) \cdot \mathbf{c}(t), \tag{1}$$

where $\mathbf{\Lambda} = \mathrm{diag}[\lambda_1, \ldots, \lambda_N] = -m\,\mathrm{diag}[\omega_1^2, \ldots, \omega_N^2]$, $\mathbf{S} = [S_{ij}]_{N\times N}$ and $S_{ij} = \varphi_i^\dagger \mathbf{V}^{(4)} \varphi_j$ is the coupling of the two normal modes under the nonlinear potential, whose absolute value characterizes the coupling strength between them. Typically, $\mathbf{V}^{(4)}$ depends on the displacements of the sites and is time-varying, and thus, S_{ij} will also be time-dependent and can actually vary significantly during the evolution. Indeed, since the elements of $\mathbf{V}^{(4)}$ are the second order polynomials of z, through the expansion $\mathbf{z} = \sum_j c_j \varphi_j$, $\mathbf{S}$ will be the second order polynomials of c_j. So, the term $\mathbf{S} \cdot \mathbf{c}$ will be cubic in the mode components.

For the graphene shown in Fig. 1(a), there are 1748 flexural modes in total, which is equal to the number of moveable atoms. Figure 1(b) shows the frequency spectrum for the graphene, where the frequencies are ordered by increasing values. Due to mirror symmetry of the system, the flexural modes are either symmetric (S) or antisymmetric (A) with respect to the x or y axis and are grouped into four different classes: symmetric-symmetric (SS), antisymmetric-symmetric (AS), SA, and AA, which is shown in Fig. 1(a) as the insets for the first four modes.

In order to characterize the relative magnitude of the three terms of the valence force potential, we calculate the potential terms $U^{(2)}$, $U_1^{(4)}$, and $U_2^{(4)}$ for the whole system under static perturbations, which is shown in Fig. 1(c). The static perturbation is on the first normal mode with different amplitudes, i.e., $z_i \sim \varphi_{1,i}$, characterized by η which is defined as the ratio of the largest deformation in the z direction to the size of the graphene sheet. In addition, the magnitude of initial deformation can also be characterized by the specific energy ϵ under the given perturbing profile, which is defined as $\epsilon = U_{sp^2}/N$. From Fig. 1(c), it can be noted that there is a cross point around $\eta \sim 0.03$, or $U \sim 10^{-20}$ J, that for small deformation ($U \ll 10^{-20}$ J), $U^{(2)}$ dominates, the system can be regarded as a harmonic oscillator with small nonlinear perturbations, and thus, the energy equipartition time can be long. While for large deformation ($U \gg 10^{-20}$ J), the system is highly nonlinear, and the energy can be easily equiparticipated.

For a given static perturbation on mode 1, Fig. 2(a) shows the coupling strength $|S_{ik}|$ between the flexural mode $k = 1$ and all the other modes at $t = 0$. It is clear that, for a given initially excited mode, only the couplings with modes

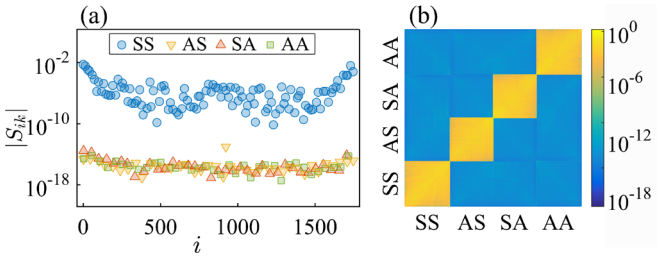

FIG. 2. (a) The coupling strength $|S_{ik}|$ between the mode $k=1$ and the other modes. The displacement profile is proportional to mode 1, and the specific energy is $\epsilon = 1.1127 \times 10^{-23}$ J. The system is 6.9 nm by 7.2 nm (1748 movable atoms). The first half modes, say $i \leq 874$, are in the acoustical branch. The last half modes ($i > 874$) are in the optical branch. For clarity reasons, not all the data points are plotted. For the modes in the same symmetry class as the initially excited one, one data point of every four is plotted, while for the modes in the other symmetry classes, one data point of every twelve is plotted. The four symmetry classes are marked by different symbols and colors. (b) For the same excitation, the contour plot of the coupling strength matrix $[|S_{ij}|]$, $i,j = 1, 2, \ldots, 1748$. The modes are reordered that those belonging to the same symmetry class are grouped together.

belonging to the same symmetry class are significant, while the values for the other modes are about 10 orders smaller, which can be neglected in the beginning of the equipartition process. Figure 2(b) shows the contour plot of the coupling strength matrix $[|S_{ij}|]$ for the same perturbation at $t=0$. The modes are reordered that those belonging to the same symmetry class are grouped together. The matrix shows clear clustered structures: the coupling strength between modes within the same symmetry class is dominantly large, e.g., about 15 orders larger than those between different symmetry classes. Although the perturbation is on the first mode, the global clustered structure is independent of this particular mode, as the coupling strength for the other clusters is in the same order of the cluster with the first mode. This forms the blockade due to the symmetry of the modes. Since the coupling characterizes the interaction strength between the modes, this would result in a quick energy flow among modes in the same symmetry class but a much slower energy flow between different symmetry classes. This has been noticed in the original FPU paper[5] that when a symmetric quartic potential is applied and the lattice is initially perturbed using an odd mode, the symmetry will be kept and only a few odd modes can be excited. Note that there are some interclass couplings that are also discernible, such as the coupling strength between mode 1 and the first few modes in the SA class as shown in Fig. 2(a). These couplings play a key role in the process of equipartition by breaking the barrier and guiding energy flow between different symmetry classes.

In our molecular dynamics (MD) simulations, the graphene sheet is initially deformed in the z direction proportional to a particular normal mode. The initial velocities are set to zero as the thermal motion has been ignored during our simulation. The MD simulation is performed using the simplified potential only considering z-displacements, where the Verlet algorithm is used for integration with a time step of 0.5 fs. The harmonic energy, i.e., the quadratic part of the energy of mode i, is given by $E_i(t) = \frac{1}{2}m(\dot{c}_i^{\,2} + \omega_i^2 c_i^2)$.[20,21] Equipartition is achieved if the energy for all the modes is comparable to each other. For most cases with large excitation energy, the system can evolve into equilibrium quickly. For some extremely low energy, the system cannot evolve into equilibrium within our computation power of 6×10^8 steps, corresponding to 300 ns.

The route to energy equipartition is mostly determined by the coupling matrix **S**. From Fig. 2, due to the symmetry blockade of **S**, this would lead to distinct time scales of energy flow among modes in the same symmetry class and those between different symmetry classes. To validate this physical picture, we calculate the harmonic energy spectrum directly during the time evolution of the system. We use the standard deviation of the modes' energy on the logarithmic scale to characterize the process towards equipartition: $\sigma(t) = \langle [\log_{10} E_i(t) - \langle \log_{10} E_i(t) \rangle]^2 \rangle^{1/2}$, where the average is over all the normal modes. A typical behavior of σ versus t for large initial energy is shown in Fig. 3(a), where the initial perturbation is on mode 1. In the beginning, $[S_{ij}]$ has finite values only for intra-class couplings, and thus, only modes in the same class of mode 1 gain energy [Fig. 3(b)]. The fine structure in S_{i1} within the class [Fig. 2(a)] is also preserved in the energy spectrum [Fig. 3(b)]. As time evolves, inter-class couplings become larger, and at time marked by (c), the strength of the coupling with class 1 has a descending order of classes 3, 2, and 4 [inset (c) of Fig. 3(a)], and thus, the modes in class 3 gain more energy [Fig. 3(c)]. However, later, the couplings between class 1 and class 4 are more significant, in a descending order of classes 4, 2, and 3 [inset (d) of Fig. 3(a)]. As a result, the energies for these three classes also follow this order [Fig. 3(d)]. The equipartition time τ is defined when $\sigma(\tau) = \sigma_{\max}/9$ and $\tau > t(\sigma_{\max})$. When equipartition is achieved [Fig. 3(e)], the clustered structure in $[S_{ij}]$ is also completely diminished [inset (e) of Fig. 3(a)].

An energy gap between the acoustical branch and the optical branch is observed in Fig. 3(c), indicating that the energy flows much easier from mode 1 to the acoustical

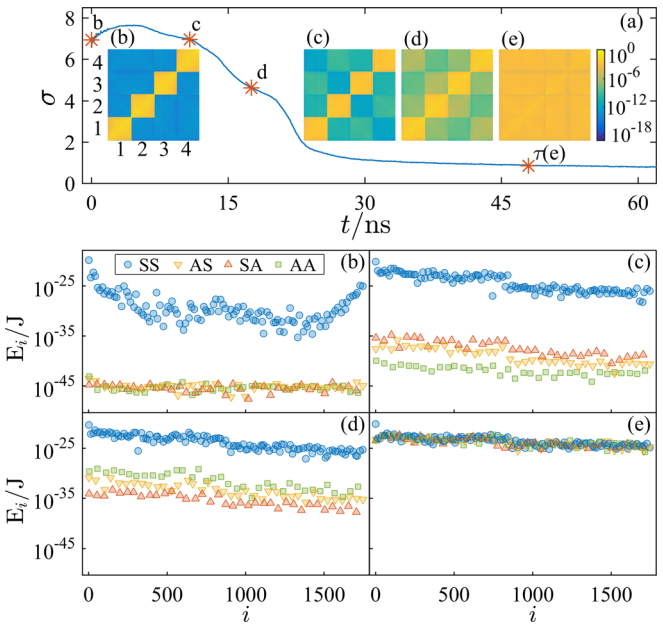

FIG. 3. (a) σ versus time. Mode 1 is excited with initial energy $\epsilon = 1.1127 \times 10^{-23}$ J. The insets show the contour plots of the matrix $[S_{ij}]$ on the log-scale at different time instances marked by (b)–(e). $[S_{ij}]$ matrix is reordered such that clusters 1–4 are for SS, AS, SA, and AA, respectively. (b)–(e) The corresponding energy spectrum at $t = 0.01$ ns, 10.79 ns, 17.55 ns, and 47.96 ns, respectively, as marked in (a). The time for (e) corresponds to the equipartition time τ.

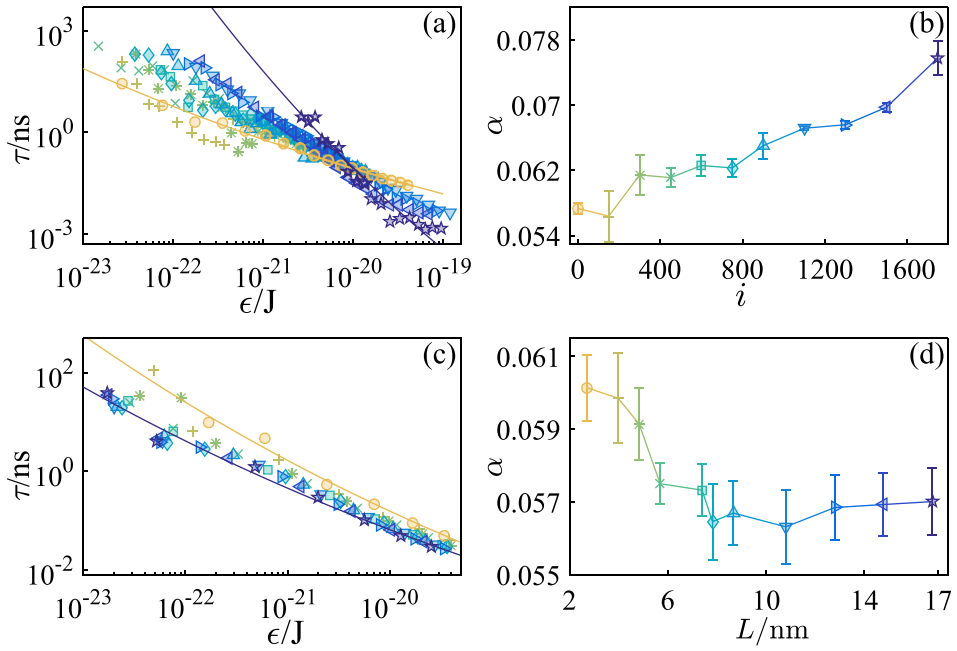

FIG. 4. (a) The equipartition time τ versus the initial specific energy ϵ for different modes of the graphene sheet in Fig. 1. Darker symbols indicate higher modes. The mode number can be readout from the horizontal label of (b), where the same symbol is for the same mode. (b) The values of α versus the mode number i. For each normal mode, α is derived by fitting the data with $\tau \sim \exp(\epsilon^{-\alpha})$. The error bar is the confidence interval during fitting. (c) τ versus ϵ for graphene sheets with different sizes. The initial deformation is on mode 1. Each type of symbol corresponds to one size, which can be readout from the horizontal label of (d). Darker symbols indicate larger graphene sheets. (d) The values of α versus the size L of the graphene sheets. The corresponding number of atoms is 296, 586, 894, 1266, 1992, 2328, 2908, 4434, 6192, 8346, and 10 820, respectively.

branch. This has been noticed by Galgani *et al.*,[22] where a model of 1D alternating masses was considered. Based on their results that the energy for the acoustic modes is far larger than that for the optical modes, it is conjectured that due to the separation of the subsystems (acoustic modes and optical modes), the energy may freeze within one subsystem, leading to nonequipartition. While for our case, although the acoustic modes are easier to get energy, it is not a dominant factor. The dominant separation of the subsystems is formed by the different symmetry classes.

It has been suggested that the equipartition time τ scales with the specific energy ϵ as $\tau \propto \exp(\epsilon^{-\alpha})$.[23–26] We have carried out extensive numerical calculations to obtain the equipartition time for different flexural modes and initial excitation energies. The results are plotted in Fig. 4(a) for the graphene sheet with 1748 free atoms. One can see that, in the loglog plot of τ versus energy ϵ, the data points do not reside on a straight line but are curved and fitted well with $\tau \sim \exp(\epsilon^{-\alpha})$. The fitted exponent α is shown in Fig. 4(b). For higher modes, the exponent becomes larger, indicating that in the small energy limit, higher modes are more difficult to reach energy equipartition. This is also evident from Fig. 4(a), which has a cross point around $\epsilon \sim 10^{-20}$ J for different modes. For larger energy, higher modes are easier to reach equipartition, while for small energies, higher modes are more difficult to reach equipartition. For example, at $\epsilon \sim 10^{-22}$ J, the equipartition time for higher modes can be a hundred times longer than that for lower modes.

An important issue which has attracted much attention is that whether the law of relaxation time could survive in the thermodynamic limit.[26,27] We have investigated graphene sheets with different sizes, with L ranging from 2.7 nm ($N = 296$) to 16.8 nm ($N = 10\,820$). Figure 4(c) shows the equipartition time for different sizes. The initial deformation is on the first mode. In general, larger systems have a smaller equipartition time, and thus, large systems are easier to get energy equipartition. In addition, as the size L increases, except the three smallest sizes (circles, pluses, and stars), the data points collapse to a single curve, indicating the convergence of the scaling in the large size limit. Figure 4(d) plots the fitting exponent α versus the system size L. α has a large value when the size is small and decreases as L increases, reaching a stable value around $L = 8$ nm. This confirms that the scaling behavior does hold in the thermodynamic limit of large systems.

It should be noted that the stretched exponential law for the equipartition time is in contrast with Ref. 27 where it is found that the relaxation time follows the $1/\epsilon$ law for a 2D lattice. This can be understood that the linear behavior of the lower part of the frequency spectrum is important for the formation of metastable states[27] that lead to the stretched exponential form for the relaxation time.[26] However, in Ref. 27, it is focused on the in-plane modes where the frequency spectrum is irregular and the linear part is lacking. As a result, although searched, the metastable states are not found. However, in our case, as shown in Fig. 1(b), the lower part of the frequency spectrum is linear, which is consistent with the dispersion relation for graphene[18] that for in-plane modes, the frequency depends linearly on the wavevector, while for the out-of-plane flexural modes, the dependence becomes parabolic at the Γ point, leading to a linear frequency spectrum and metastable states.[6,28] This justifies the stretched exponential form in our case.

To conclude, we have investigated the interactions between the flexural modes due to nonlinear potentials in square graphene resonators. The flexural modes are divided into different classes owing to their symmetries. It is found that the intra-class interactions are significantly stronger than inter-class

interactions. Therefore, the modes belonging to the same symmetry class as the initially excited one can be easily excited, while modes in different symmetry classes will be blocked, especially in the beginning of the evolution of the system. However, as time evolves, more and more modes are excited, and the displacement profile becomes complex such that the interaction between modes in different symmetry classes also becomes large, and then, the inter-class blockade can be broken, leading to final equipartition. Because of the existence of symmetry blockades, phonon-phonon scattering between different symmetry classes is significantly suppressed, providing a similar mechanism to reduce the phase space for allowed anharmonic phonon-phonon scattering as observed in Ref. 29, contributing to the high thermal conductivity of graphene. The relaxation time follows the stretched exponential law and survives in the thermodynamic limit. The dependence of the relaxation time on the system size may be helpful to understand the superanomalous heat conduction[13] in graphene, but it needs further in-depth studies to clarify the detailed relation. Therefore, our results have revealed the dynamical organization and the route to equipartition of the flexural modes, which are important to the understandings of the flexural modes and their peculiar contributions to the high heat conductivity and to the understanding of the energy dissipation mechanism due to anharmonic phonon-phonon scattering.

We thank Professor H. Zhao, Professor L. Rondoni, and Professor G. Casati for illuminating discussions. This work was supported by the NNSF of China under Grant Nos. 11335006, 11375074, 11422541, and 11775101, by the President Foundation of Xiamen University under Grant No. 20720150036, and by the Fundamental Research Funds for the Central Universities under Grant No. lzujbky-2016-k05.

[1]J. S. Bunch, A. M. van der Zande, S. S. Verbridge, I. W. Frank, D. M. Tanenbaum, J. M. Parpia, H. G. Craighead, and P. L. McEuen, Science **315**, 490 (2007).
[2]C. Lee, X. Wei, J. W. Kysar, and J. Hone, Science **321**, 385 (2008).
[3]R. A. Barton, B. Ilic, A. M. van der Zande, W. S. Whitney, P. L. McEuen, J. M. Parpia, and H. G. Craighead, Nano Lett. **11**, 1232 (2011).
[4]A. A. Balandin, Nat. Mater. **10**, 569 (2011).
[5]E. Fermi, J. Pasta, and S. Ulam, Technical Report No. LA-1940, Los Alamos Scientific Laboratory, Los Alamos, 1955.
[6]D. Midtvedt, A. Croy, A. Isacsson, Z. Qi, and H. S. Park, Phys. Rev. Lett. **112**, 145503 (2014).
[7]J. H. Seol, I. Jo, A. L. Moore, L. Lindsay, Z. H. Aitken, M. T. Pettes, X. Li, Z. Yao, R. Huang, D. Broido, N. Mingo, R. S. Ruoff, and L. Shi, Science **328**, 213 (2010).
[8]F. Izrailev and B. Chirikov, Dokl. Akad. Nauk SSSR **166**, 57 (1966) [Sov. Phys. Dokl. **11**, 30 (1966)].
[9]F. Izrailev, A. Khisamutdinov, and B. Chirikov, Report 252, Institute of Nuclear Physics, Novosibirsk, USSR, 1968 (English translation: LA-4440-TR, Los Alamos, 1970).
[10]N. Sait, N. Hirotomi, and A. Ichimura, J. Phys. Soc. Jpn. **39**, 1431 (1975).
[11]D. S. Sholl and B. I. Henry, Phys. Lett. A **159**, 21 (1991).
[12]D. S. Sholl and B. I. Henry, Phys. Rev. A **44**, 6364 (1991).
[13]A. Lippi and R. Livi, J. Stat. Phys. **100**, 1147 (2000).
[14]C. Chen, S. Rosenblatt, K. I. Bolotin, W. Kalb, P. Kim, I. Kymissis, H. L. Stormer, T. F. Heinz, and J. Hone, Nat. Nanotechnol. **4**, 861 (2009).
[15]A. Eichler, J. Moser, J. Chaste, M. Zdrojek, I. Wilson-Rae, and A. Bachtold, Nat. Nanotechnol. **6**, 339 (2011).
[16]P. N. Keating, Phys. Rev. **145**, 637 (1966).
[17]R. M. Martin, Phys. Rev. B **1**, 4005 (1970).
[18]C. Lobo and J. Łułs, Z. Phys. D **39**, 159 (1997).
[19]J. Atalaya, A. Isacsson, and J. M. Kinaret, Nano Lett. **8**, 4196 (2008).
[20]G. Berman and F. Izrailev, Chaos **15**, 015104 (2005).
[21]H. J. Matsuyama and T. Konishi, Phys. Rev. E **92**, 022917 (2015).
[22]L. Galgani, A. Giorgilli, A. Martinoli, and S. Vanzini, Physica D **59**, 334 (1992).
[23]N. N. Nekhoroshev, Russ. Math. Surv. **32**, 1 (1977).
[24]G. Benettin, L. Galgani, and A. Giorgilli, Celest. Mech. **37**, 1 (1985).
[25]M. Pettini and M. Landolfi, Phys. Rev. A **41**, 768 (1990).
[26]L. Berchialla, A. Giorgilli, and S. Paleari, Phys. Lett. A **321**, 167 (2004).
[27]G. Benettin, Chaos **15**, 015108 (2005).
[28]Y. Wang, Z. Zhu, Y. Zhang, and L. Huang, Phys. Rev. E **97**, 012143 (2018).
[29]L. Lindsay, D. A. Broido, and N. Mingo, Phys. Rev. B **82**, 115427 (2010).